

Effects of Disorder and Momentum Relaxation on the Intertube Transport of Incommensurate Carbon Nanotube Ropes and Multiwall Nanotubes

M. A. Tunney and N.R. Cooper

*T.C.M. Group, Department of Physics Cavendish Laboratory,
J. J. Thomson Avenue, Cambridge CB3 0HE, United Kingdom.*

(Dated: 1 May 2006)

We study theoretically the electrical transport between aligned carbon nanotubes in nanotube ropes, and between shells in multiwall carbon nanotubes. We focus on transport between two metallic nanotubes (or shells) of different chiralities with mismatched Fermi momenta and incommensurate periodicities. We perform numerical calculations of the transport properties of such systems within a tight-binding formalism. For clean (disorder-free) nanotubes the intertube transport is strongly suppressed as a result of momentum conservation. For clean nanotubes, the intertube transport is typically dominated by the loss of momentum conservation at the contacts. We discuss in detail the effects of disorder, which also breaks momentum conservation, and calculate the effects of localised scatterers of various types. We show that physically relevant disorder potentials lead to very dramatic enhancements of the intertube conductance. We show that recent experimental measurements of the intershell transport in multiwall nanotubes are consistent with our theoretical results for a model of short-ranged correlated disorder.

PACS numbers: 73.63.Fg, 73.22.-f, 72.10.-d

I. INTRODUCTION

The electronic properties of carbon nanotubes are the source of much very interesting physics. Not only are carbon nanotubes highly one-dimensional conductors, but the dependence of the nanotube bandstructure on the nanotube's "chirality" leads to a range of different bandstructures: both metallic and semiconducting behaviours arise and, even within each of these, the possible bandstructures vary considerably.¹ The nature of the bandstructure has important effects on the electronic transport properties, not least the large difference in the effects of disorder on metallic nanotubes as compared to (doped) semiconducting nanotubes.^{2,3,4}

Theory shows that the bandstructure also plays key roles in the intertube transport between (the outer shells of) aligned nanotubes in a rope,⁵ and in the transport between the shells of a multiwall nanotube (MWNT).⁶ [Henceforth, we shall discuss these two cases together by referring to the transport as *intertube* transport, with the two "tubes" to be understood as single-wall nanotubes (SWNTs) representing either the outer shells of two neighbouring nanotubes in a nanotube rope, or two neighbouring shells in a MWNT.] In experimental systems of this type, the two tubes typically have differing chiralities and therefore differing bandstructures. Even when the two tubes are both metallic, the typical case poses a complicated situation: the Fermi momenta do not coincide, and their translational periods are incommensurate. Consequently, as a result of momentum conservation, one expects a strong suppression of intertube tunnelling⁵ as compared to the simplest case of two identical tubes (with matched Fermi momenta and commensurate periodicity). Indeed, theory has led to the counter-intuitive prediction that increasing the length over which the two shells of a MWNT are coupled will *reduce* the

intershell conductance.⁶

A knowledge of the intertube conductance in nanotubes ropes and intershell conductance in MWNTs is of fundamental importance for understanding the transport mechanisms in these systems. However, direct experimental studies of these quantities cannot easily be achieved. Very elegant recent experimental work has succeeded in probing the intertube/shell conductivity. Experimental studies on intentionally disordered nanotube ropes⁷ have been used to estimate the intertube tunnelling conductance. Non-local resistance measurements between contacts on the outer shells of MWNTs have been used to determine the intershell conductivity.⁸ (The development of telescopically extended MWNTs⁹ opens the way to future studies of intershell conductance. However, at present the transport properties appear not to be dominated by the intershell conductance.⁹)

As emphasised in Ref. 8, the experimental measurements of intershell transport in MWNTs cannot be accounted for within existing theories. The experimental systems have some degree of disorder, and existing theories do not take disorder into account. Disorder is likely to have a very dramatic effect on the intertube/shell transport: disorder breaks translational symmetry and therefore relaxes the momentum conservation which is responsible for the suppression^{5,6} of intertube transport.

In this paper, we report calculations of the effects of disorder on the intertube conductance in carbon nanotube ropes and MWNTs. In the rope geometry, we consider two nearest-neighbour tubes and study the transport between the outer shells of these tubes. In the multiwall geometry (in which the shells are coaxial) we study the transport between two neighbouring shells of the tube [thus we effectively consider a double wall nanotube (DWNT)]. We focus on two metallic shells of armchair and zigzag type, which provides an example of the

typical case involving mismatched Fermi momenta and incommensurate periodicities. We show that defects lead to very dramatic *enhancements* of the intertube conductance. We quantify the effects of defects of different types, and discuss the results in connection with experimental results of Refs. 7 and 8. Our results show that disorder has a large effect for both the intertube transport in disordered ropes measured in Ref. 7, and for the intershell transport in MWNTs measured in Ref. 8. By comparing our theory to the experimentally determined intershell conductance of MWNTs⁸ we put constraints on the nature of the disorder in these samples, and find parameter regimes of disorder for which our theoretical results are consistent with the experimental measurements.⁸

The paper is organised as follows. In §II we describe the model that we use, and discuss the importance of translational and rotational symmetries in the intertube coupling in aligned carbon nanotubes. We introduce a classification of the coupling strength between two shells of a MWNT based on the rotational symmetry. In §III we describe the Green's function approach used in our numerical studies. In §IV we apply this to the case of clean (disorder-free) nanotubes. We demonstrate the importance of momentum conservation for clean nanotubes. We show that momentum-relaxation at the contacts is the dominant effect controlling the intertube transport in clean nanotubes. The importance of our classification of the rotational symmetry in MWNTs is demonstrated through calculations of transport between nanotube shells in a telescopic junction geometry. In §V we turn to study the effects of disorder on the intertube conductance. We calculate the effects of localised defects of different types, and compare our results to the experimental measurements of Refs. 7 and 8. Finally in §VI we summarise the main results of the paper.

While preparing this work for publication, we learned of related work¹⁰ where the importance of momentum relaxation at the contacts of clean DWNTs was also recognised. Since our discussion of this aspect in §IV is somewhat different from Ref. 10, and since an understanding of the clean case is required in order to introduce our calculations of the effects of defects, we retain this discussion. Our results in this section are consistent with those of Ref. 10.

II. NANOTUBE BANDSTRUCTURES, TRANSLATIONAL AND ROTATIONAL SYMMETRIES

A. Theoretical Model

We describe the bandstructure of the nanotubes using a one-band tight binding Hamiltonian,

$$\mathcal{H}_0 = -t \sum_{\langle i,j \rangle, \sigma} (c_{i\sigma}^\dagger c_{j\sigma} + c_{j\sigma}^\dagger c_{i\sigma}) \quad (1)$$

where $c_{i\sigma}$ and $c_{i\sigma}^\dagger$ are the annihilation and creation operators for an electron with spin polarisation $\sigma = \pm 1/2$ on the atomic site i . The atoms lie on a (rolled up) honeycomb lattice, with lattice constant $a = 2.46\text{\AA}$ and hopping occurring only between nearest neighbour sites $\langle i, j \rangle$. For quantitative estimates, we use $t = 2.77\text{eV}$ consistent with the value fitted to the results of tunnelling experiments.¹¹

We consider intertube conductance between two carbon nanotubes due to the addition of a tunnelling Hamiltonian

$$\mathcal{H}_T = - \sum_{j,i,\sigma} t_{ij} (c_{i\sigma}^\dagger c_{j\sigma} + c_{j\sigma}^\dagger c_{i\sigma}) \quad (2)$$

where i and j now label atomic sites on two different tubes. Following Ref. 5, we model the intertube hopping (between atoms at positions \mathbf{r}_i and \mathbf{r}_j) by

$$t_{ij} = t_\perp e^{-|\mathbf{r}_i - \mathbf{r}_j|/\delta} \quad (3)$$

with $t_\perp = 492\text{eV}$ and $\delta = 0.5\text{\AA}$. We have also performed calculations (not reported here) using a more sophisticated model¹³ which accounts for the angular dependence of the hopping through σ and π bonds. We find similar results using either parameterisation in all cases we have studied (with realistic geometries). For the purposes of this paper, we therefore restrict attention to the results of the simpler model (3).

In all the calculations we report, we treat the electrons as non-interacting. The results are thus valid at high temperatures, or for systems with many occupied modes, as in MWNTs, where the effects of interactions are suppressed. We discuss briefly the influence of interactions in §VI.

B. Bandstructures of Armchair and Zigzag Nanotubes

It is well-known that the electronic properties of carbon nanotubes depend on the chiral vector (n_1, n_2) , which sets the quantised subbands and thus the bandstructure.¹ In this work we focus on metallic armchair and zigzag nanotubes.

Armchair tubes are described by (n_a, n_a) chiral vectors. The wavevector around the tube circumference takes the values $k_\perp = (2\pi/\sqrt{3}a)(q/n_a)$ with $q = 1, 2, \dots, 2n_a$. For each q there are two bands, labelled by \pm , which have the energy dispersions

$$\epsilon_q^{\text{ac}}(k) = \pm t \left[1 + 4 \cos\left(\frac{q\pi}{n_a}\right) \cos\left(\frac{ka}{2}\right) + 4 \cos^2\left(\frac{ka}{2}\right) \right]^{\frac{1}{2}} \quad (4)$$

where k is the wavevector k along the tube, with $-\pi < ka < \pi$. The \pm bands with $q = n$ are metallic, crossing $E = 0$ at $k = \pm 2\pi/(3a)$.

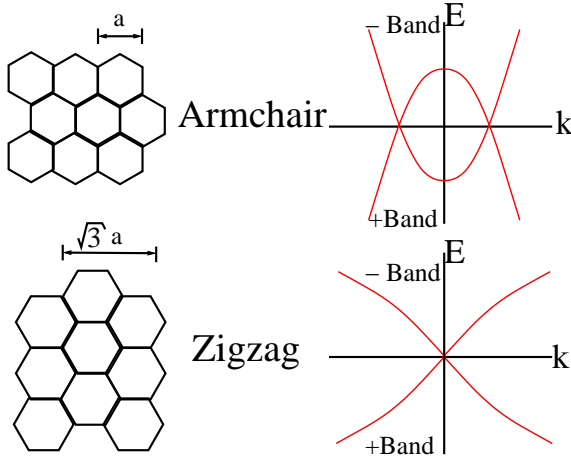


FIG. 1: (Color online) Schematic diagrams of the lattice structures (the tube axes run horizontally) and bandstructures of the metallic bands for armchair and zigzag nanotubes. The repeat distances along the tube axes differ by a factor of $\sqrt{3}$, so the tubes are incommensurate. Intertube tunnelling will be suppressed for Fermi energies close to $E = 0$, owing to the lack of energy-momentum conserving processes.

Zigzag tubes are described by $(n_z, 0)$ chiral vectors. The wavevector around the tube circumference takes values $k_\perp = (2\pi/a)(q/n_z)$, with $q = 1, \dots, 2n_z$, and the subbands have dispersion relations

$$\epsilon_q^{zz}(k) = \pm t \left[1 + 4 \cos\left(\frac{\sqrt{3}ka}{2}\right) \cos\left(\frac{q\pi}{n_z}\right) + 4 \cos^2\left(\frac{q\pi}{n_z}\right) \right]^{\frac{1}{2}} \quad (5)$$

with $-\pi/\sqrt{3} < ka < \pi/\sqrt{3}$. If n_z is an integer multiple of 3, the zigzag tube is metallic. The metallic subbands have $q = 2n_z/3, 4n_z/3$ (the \pm bands correspond to right- and left-moving modes of these two subbands). The two metallic subbands both cross $E = 0$ at $k = 0$.

The lattice structures and metallic bands of armchair and zigzag nanotubes are illustrated in Fig. 1.

C. Intertube Conductance: Momentum Conservation and Incommensurability

We explore the effects of momentum (wavevector) conservation in the intertube conductance between two aligned nanotubes. First, in order to explain the importance of momentum conservation, we consider the tubes to be sufficiently weakly coupled that this coupling can be described by perturbation theory. This is valid provided the intertube conductance is small compared to e^2/h . (Our numerical results will not be restricted to this perturbative limit.) Within perturbation theory, for transport between a Fermi point k_A on one tube and a Fermi point k_B on the other there is a contribution to

the intertube conductance of

$$G_{k_A, k_B} = \frac{2e^2}{\hbar^3 v_A v_B} \frac{L_N^2}{2\pi} |t_{k_A k_B}|^2 \quad (6)$$

where

$$t_{k_A k_B} \equiv \langle k_B | \mathcal{H}_T | k_A \rangle \quad (7)$$

is the tunnelling matrix element, v_A and v_B are the velocities at the two Fermi points, and L_N is the length over which the states $|k\rangle$ are normalised. The total conductance is obtained by the sum of (6) over all initial and final Fermi points (k_A, k_B) associated with the different occupied subbands [we have suppressed band indices in Eqs. 6 and 7].

Momentum conservation arises from the symmetry of the tunnelling Hamiltonian (3) under translation along the tube.¹² If the Fermi momenta of the two tubes are the same, ($k_A = k_B$), then electrons at the Fermi energy can tunnel between the tubes conserving both energy and momentum: one expects a large intertube conductance. (For two tubes of the same type, the Fermi momenta coincide at all energies so intertube coupling is always strong.) If the Fermi momenta differ ($k_A \neq k_B$), tunnelling will be suppressed. In general, tubes of different chiralities have different dispersion relations and therefore differing Fermi momenta. For example, as shown in Fig. 1, the Fermi momenta of the armchair and zigzag tubes differ in a range of Fermi energies around $E = 0$. (At $E_F = 0$ the Fermi momenta are $k_F^{ac} = \pm 2\pi/(3a)$ and $k_F^{zz} = 0$ for armchair and zigzag tubes respectively.)

Although one might conclude that if the Fermi momenta differ, intertube tunnelling will vanish identically, this is not always true. An important distinction arises between the cases in which the tubes have *commensurate* or *incommensurate* lattice structures. Denoting the repeat distances in the two tubes by a_A and a_B , we say that the carbon nanotubes are commensurate if a_A/a_B is rational fraction, and that they are incommensurate if this is an irrational fraction.

If the carbon nanotubes are *commensurate*, then the system has translational symmetry along its length. The minimum distance along the tubes under which the system is translationally invariant sets the size of the first Brillouin zone. If the Fermi momenta of the two tubes do not coincide within this first Brillouin zone, then there can be no tunnelling between the tubes that conserves energy and (crystal) momentum. The intertube tunnelling will vanish.

If the carbon nanotubes are *incommensurate*, then there is no finite distance under which the system is translationally invariant: the size of the first Brillouin zone is vanishingly small, and the eigenstates cannot be characterised by a conserved crystal momentum. Nevertheless, for weak coupling between the tubes, the Bloch states of the individual tubes still provide a useful starting point. Imagine that, in the first Brillouin zones of the individual tubes, the Fermi momenta of the two tubes do

not coincide. Because the reciprocal lattice vectors are incommensurate, by adding sufficient reciprocal lattice vectors to each of the tubes one will be able to bring the Fermi momenta arbitrarily close. (That is, in an extended zone scheme the Fermi momenta can become arbitrarily close.) However, as shown by Maarouf *et al.*⁵, the larger the number of reciprocal lattice vectors that must be added to achieve momentum matching, the weaker is

$$t_{\mathbf{k}^A, \mathbf{k}^B} = t_{\perp} \delta_{k_*^A, k_*^B} \sqrt{\frac{2\pi}{b+2R} \frac{b\delta^{\frac{3}{2}}}{A_{\text{cell}}}} e^{-b/\delta} e^{-b\delta K^2/2} e^{-(k_{\perp}^A - k_{\perp}^B)^2 R\delta/4} e^{-Rb\delta(k_{\perp}^A + k_{\perp}^B)^2/4(b+2R)} \quad (8)$$

where A_{cell} is the area of a unit cell, $k_{\perp}^{A,B}$ are the (subband) wavevectors around the tube circumference, $k_*^A \equiv k^A + \alpha G^A$ and $k_*^B \equiv k^B + \beta G^B$ are the wavevectors along the tubes shifted by integer numbers (α, β) of reciprocal lattice vectors along the tube (G^A, G^B), $K^2 \equiv |k_*^A|^2 + |k_*^B|^2$, and b is the distance between tubes at the point of closest approach. For larger numbers of reciprocal lattice vectors, K^2 increases and the tunnelling matrix element is exponentially suppressed. One expects the tunnelling to be dominated by processes involving the smallest number of additional reciprocal lattice vectors.⁵

Two tubes of different chiralities typically have Fermi momenta that do not coincide, and typically are incommensurate. The armchair and zigzag tubes are an example of this typical case. Here, the smallest reciprocal lattice vectors are $G^{ac} = 2\pi/a$, $G^{zz} = 2\pi/\sqrt{3}a$. The condition for energy-momentum conservation is

$$\epsilon_{q_a}^{ac} (k_F^{ac} + \alpha G^{ac}) = \epsilon_{q_z}^{zz} (k_F^{zz} + \beta G^{zz}) = E_F \quad (9)$$

where $k_F^{ac/zz}$ are the Fermi momenta along the respective tube axes, and α and β are integers. Focusing on the dominant tunnelling process involving just one reciprocal lattice vector of each tube, we look for a solutions with $\alpha = \pm 1$ and $\beta = \pm 1$. Using the dispersion relations (4,5) we find $ka = \pm 3.914$ at energies $E_F = \pm E_0$ where $E_0 = 0.247t$. We shall show the importance of this energy in the numerical results in §IV B.

D. Multiwall Geometry: Rotational Symmetry

In the case of MWNTs, intertube conductance is strongly affected not only by momentum conservation along the tube, but also by angular momentum conservation around the axis of the tube. This leads to additional selection rules in the tunnelling matrix elements which depend sensitively on the chiralities of the two tubes.^{6,14}

We discuss the implications of this symmetry for the tunnelling matrix element (7) between armchair and zigzag shells. The subband wavefunctions vary as $e^{ik_{\perp}y}$,

the tunnelling between the two tubes. Ref. 5 provided an approximate calculation of the matrix element of the intertube coupling (2) between momentum eigenstates on two aligned nanotubes placed side-by-side (as in a carbon nanotube rope). Following this approach,⁵ which is valid in the limit that tunnelling is dominated by the points of closest approach, we find that the matrix element is

where y is the coordinate around the circumference of the tube. For an (n_a, n_a) armchair tube, $k_{\perp} = 2\pi/(\sqrt{3}a)(q_a/n_a)$, and the lattice is invariant under a translation by $\sqrt{3}a$ in y . Using $\theta_i^a = y_i/(\sqrt{3}an_a) = i/n_a$ to label the angular position of the unit cell i ($i = 1, \dots, n_a$), then the subband wavefunction is simply $e^{iq_a \theta_i^a}$. Similarly for the zigzag tube, $\theta_j^z = y_j/(an_z) = j/n_z$, and the subband wavefunction is $e^{iq_z \theta_j^z}$ for the unit cell labelled by $j = 1, \dots, n_z$. Therefore, the tunnelling matrix element contains an angular contribution of the form

$$\begin{aligned} \langle \Psi_z | \mathcal{H}_T | \Psi_a \rangle &\propto \sum_{i,j} \tilde{t}(\theta_i^a - \theta_j^z) e^{iq_a \theta_i^a} e^{-iq_z \theta_j^z} \\ &= \sum_{i,j} \sum_n \tilde{t}_n e^{-in(\theta_i^a - \theta_j^z)} e^{iq_a \theta_i^a} e^{-iq_z \theta_j^z} \end{aligned}$$

where $\tilde{t}(\theta_i^a - \theta_j^z)$ is the function obtained by expressing (3) in terms of the angular separation between atoms in the two shells, which in the last line has been expressed as a Fourier series due to its periodicity. Performing the sums over i and j , one finds that the contribution of the harmonic \tilde{t}_n is nonzero only if

$$\text{Condition A: } \text{mod}(n - q_a, n_a) = 0 \quad (10)$$

$$\text{Condition B: } \text{mod}(n - q_z, n_z) = 0 \quad (11)$$

If both of these conditions are met, then modes q_a and q_z are connected by a non-zero tunnelling matrix element. Restricting attention, now, to the metallic bands in both tubes – that is, $q_a = n_a$ and $q_z = 2n_z/3$ or $q_z = 4n_z/3$ – the conditions (11) may be rewritten

$$\text{A: } n = \alpha n_a$$

$$\text{B: } n = n_z \left(\frac{1}{3} + \beta \right) \quad \text{or} \quad n = n_z \left(\frac{2}{3} + \beta \right)$$

We classify the nature of the rotational symmetry of the tubes in three cases. Which case applies depends on the ratio $n_a/n_z = p/q$ where p and q are natural numbers with no common factor.

(i) “Zero”: No value of n that satisfies condition B satisfies A. This is the case if q is not divisible by 3. The

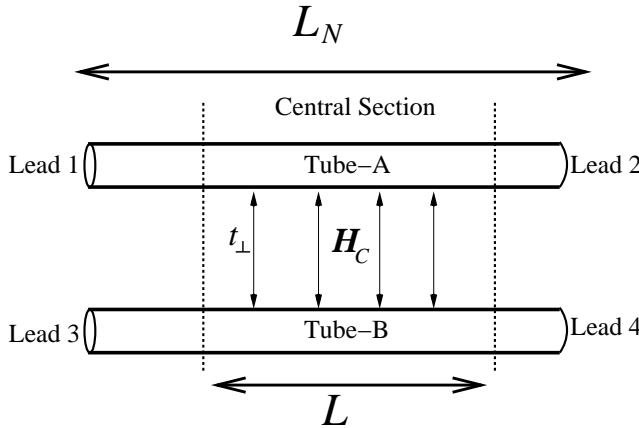


FIG. 2: Geometry of the system that we study, illustrating the labelling of the leads and the length L of the central section where intertube tunnelling can occur. The length L_N , which includes the leads, is used for normalisation and is assumed large.

tunnelling matrix elements between the metallic bands of the armchair and zigzag tubes vanish identically.

(ii) **“Strong”**: All values of n that satisfy condition B, satisfy A. This is the case if q is divisible by 3 and if $p = 1$. The metallic bands of the armchair and zigzag tubes couple strongly, containing contributions from all possible angular harmonics of the tunnelling operator.

(iii) **“Intermediate”**: Some values of n that satisfy condition B satisfy A. This is the case if q is divisible by 3 and if $p \neq 1$. The metallic bands of the armchair and zigzag tubes are coupled, but contain contributions from only a subset of the angular harmonics of the tunnelling operator.

That rotational symmetry can lead to vanishing matrix elements (the “zero” case) is well-known.^{6,14} However, as we show below in our numerical results, there can be very substantial quantitative differences between cases we discriminate as “intermediate” or “strong” coupling.

III. CONDUCTANCE USING GREEN’S FUNCTIONS

In our numerical studies, we calculate the conductance of the double nanotube system within the Landauer-Büttiker framework, with the scattering matrix calculated numerically using a Green’s function approach.¹⁵ The geometry of the system studied is shown in Fig. 2. It consists of two parallel nanotubes, each of which we shall consider to be either armchair or zigzag type. The geometry allows a description of (the outer shells of) two neighbouring tubes in a rope geometry (if the tube axes do not coincide), or two neighbouring shells in a MWNT (if the axes do coincide).

We calculate the conductance using a scattering approach. For this purpose, we consider leads to be attached to the ends of each nanotube. The leads are ideal,

consisting of a semi-infinite section of clean nanotube, and there is no intertube coupling between the leads. The intertube coupling is confined to the central section of length L . In this region the system has Hamiltonian \mathcal{H}_C , which describes atomic sites that experience intra- and inter-tube hopping and where there can be diagonal or off diagonal disorder. The nature of the intertube scattering in this region determines if we are considering the rope or multiwall geometry.

Following the approach described in Ref. 15, the overall Green’s function at energy E can be obtained via a matrix inversion

$$\mathcal{G}_C = [E\mathcal{I} - \mathcal{H}_C - \Sigma]^{-1} \quad (12)$$

where the matrix has dimension $C \times C$, with C the number of sites in the central region. [The typical system sizes we study have on the order of $C = 9000$ atoms. Matrix inversion is done using standard LaPack code.] The effects of the leads are taken into account via a self-energy term $\Sigma = \sum_p \tau_p^\dagger g_p \tau_p$ which can be viewed as an effective Hamiltonian describing the coupling between the conductor and the four leads (labelled by $p = 1, \dots, 4$). In this expression, g_p is the end Green’s function of lead p and τ_p is a matrix describing the coupling of this lead to the central region. Although the leads are semi-infinite, the end Green’s function has finite dimension, set by the number of sites on the end of the lead.

We restrict attention to the case in which the energy is sufficiently close to $E = 0$ that there are only two conducting modes in each of the metallic nanotube leads. This allows a description of transport properties when the energy E is less than the gap to the next subband. In this case, it is sufficient to calculate the Green’s function for the leads including only these metallic modes. We have determined the end Green’s function analytically for the metallic modes of the armchair and zigzag tubes (the calculation is described in Appendix VII), allowing an analytic determination of the self-energy entering Eqn. 12. Note that in the “central” region the system is solved fully (numerically), including all subbands.

For the range of energy that we study, the transmission matrix is an 8×8 matrix, $T_{\mu,p;\mu',p'}$, describing the transmission from two incoming modes (labelled by μ) in each of the four leads ($p = 1, 2, 3, 4$) to the 2×4 outgoing modes (with mode μ' and lead p'). The nature of the mode depends on whether the lead is of armchair or zigzag type: for an (n_a, n_a) armchair tube, μ labels the \pm bands with $q_a = n_a$; for a $(0, n_z)$ zigzag tube, μ labels $q_z = 2n_z/3, 4n_z/3$. We obtain the scattering matrix for currents, following the approach described in Ref. 15 for a continuum system applied to this discrete case. As in the case of the continuum, it is important to convert the matrix for scattering amplitudes into the matrix for scattering fluxes using the velocities of the initial and final modes. From the scattering amplitude for the flux, one obtains the transmission probabilities, the final results for which are given in Appendix VIII.

Finally, using the Landauer-Büttiker approach, the

conductance is obtained from the sum of the transmission probabilities. For example, the intertube conductance between tube-A ($p = 1, 2$) and tube-B ($p = 3, 4$) as measured in an experiment with contacts attached to all four leads, involves the total transmission coefficient between all modes in the tube-A and all modes in tube-B

$$G = \frac{2e^2}{h} \sum_{\mu; p=1,2} \sum_{\mu'; p'=3,4} T_{\mu,p; \mu',p'} \quad (13)$$

The prefactor of 2 arises from spin degeneracy. The maximum intertube conductance in this case is $8e^2/h$.

A. Application: Conductance of a SWNT with a Vacancy

As a first application of our numerical method, we study the two-terminal conductance of *single* SWNTs (both armchair and zigzag) in the presence of a vacancy. This is achieved simply by turning off intertube tunnelling, $t_{\perp} = 0$, and calculating the scattering between the two ends of the individual tubes. Thus, the two-terminal conductance of tube-A is

$$G_{\text{intra}} = \frac{2e^2}{h} \sum_{\mu, \mu'} T_{\mu,1; \mu',2}$$

which has maximal value $4e^2/h$ for a clean metallic nanotube (two propagating modes and twofold spin degeneracy).

Related calculations of the effects of vacancies on armchair SWNTs have been reported previously.^{16,17,18,19} As in those studies we do not include relaxation of the lattice around the vacancy, but leave the honeycomb lattice undistorted. Following Ref. 19 we model the vacancy by imposing a huge potential on the vacancy site (10^8 eV), which was shown¹⁹ to be equivalent to explicit disconnection of the bonds to this site.

In Fig. 3 we present results for the conductance of single metallic armchair and zigzag carbon nanotubes in the presence of a single vacancy. Our calculations reproduce the results previously found by Igami *et al.*¹⁹ for armchair tubes. In addition, we present results for a metallic zigzag nanotube. The results in both cases (armchair and zigzag) are very similar: the conductance drops from close to its ideal value of $4e^2/h$ at the edge of the second conduction band, to $2e^2/h$ at $E = 0$.²⁰

One can understand that the minimum value of the conductance at $E = 0$ is $G_{\text{intra}} = 2e^2/h$ by noting that, in both armchair and zigzag cases, a linear combination of the two degenerate right-moving (or left-moving) states of an ideal (defect free) nanotube can be formed that has zero amplitude on a subset of the lattice sites. Choosing the linear combination such that the amplitude is zero on the site containing the vacancy, this mode of the ideal tube is unaffected by the presence of a vacancy and therefore contributes $2e^2/h$ to the two-terminal conductance.

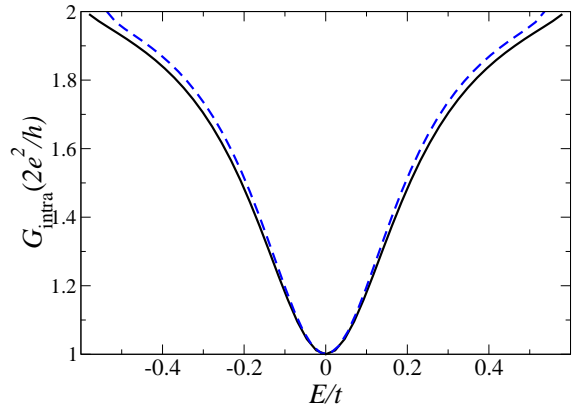


FIG. 3: (Color online) Two-terminal conductance of a (5,5) armchair nanotube with a single vacancy (solid line) and a (9,0) nanotube with a single vacancy (dashed line). The tube length ($L = 31a$) used in these calculations is sufficiently long that the results are characteristic of the bulk behaviour.

That our numerical results show that the conductance falls to precisely this minimum value at $E = 0$ indicates that the other (orthogonal) mode is completely reflected by the vacancy. For an armchair tube, the wavefunction of the transmitted mode is periodic along the length of the tube every three lattice constants [it is a superposition of waves with $k = +2\pi/(3a)$ and $k = -2\pi/(3a)$]. Therefore, one expects that it should be possible to introduce several vacancies, at positions chosen judiciously to lie at the set of zeroes of this transmitted mode, without having any effect on its transmission. We have checked this expectation numerically by introducing several vacancies in the carbon nanotube on sites respecting the periodicity of the wavefunction: at $E = 0$ the conductance remains $2e^2/h$, indicating that the transmitted wave indeed does not feel the potentials on these sites.

IV. INTERTUBE CONDUCTANCE BETWEEN TWO CLEAN SWNTS

We now turn to consider the intertube conductance between aligned nanotubes in both rope and multiwall geometries. From the discussions of §II C we expect that momentum conservation and, in the case of MWNTs, the rotational symmetry will play important roles in determining the magnitude of the intertube conductance. Here, we investigate these effects, focusing on the case of clean tubes in the absence of defects. A discussion of the effects of defects will be given in §V. We begin our discussion by considering the effects of the loss of momentum conservation at the contacts.

A. Contact Effects

The presence of current contacts at the two ends of a carbon nanotube sets a finite total length of the system,

L . In Ref. 6 it was recognised that as a consequence of this finite length, L , momentum conservation will be relaxed on a wavevector scale of order $1/L$. This led to the prediction⁶ of a decrease in the intershell conductance of a MWNT with increasing length L , as momentum conservation becomes more accurately satisfied.

Another effect is that in the vicinity of the contacts themselves the translational symmetry is broken. We denote the (minimum) intrinsic lengthscale of the contact L_c : this could be the size of the contact, or the lengthscale over which the electronic nanotube density changes between a region under the contact and a region away from the contact. The variation of the nanotube properties on L_c will promote a loss of momen-

tum conservation up to a wavevector scale of about $1/L_c$. Since $1/L_c \gg 1/L$, this change in momentum will typically be larger than that arising from the finite length of the tube. We find that momentum relaxation at the contacts typically dominates the transport properties between clean nanotubes with mismatched Fermi momenta. The contact-induced contribution to the intertube conductance was not considered in Ref. 6.

Since we are interested in the general features of momentum (non-) conservation at the contacts, we introduce a simple model that incorporates a contact lengthscale L_c as well as the total length L . Specifically, we replace (2) by

$$t_{ij} = t_{\perp} e^{-|\mathbf{r}_i - \mathbf{r}_j|/\delta} \times f\left(\frac{x_i - L}{L_c}\right) \times f\left(-\frac{x_i}{L_c}\right) \times f\left(\frac{x_j - L}{L_c}\right) \times f\left(-\frac{x_j}{L_c}\right) \quad (14)$$

where $f(x) \equiv 1/(e^x + 1)$ and x_i, x_j are the distances along the two tubes. This describes intertube tunnelling over a total length L , but with the tunnelling rising smoothly over a lengthscale L_c from zero (far inside the “leads”) to its maximal value. Although this model for smooth contacts (14) does not accurately mimic experimental situations, it provides a convenient way in which to control the extent of scattering at the contacts. We shall make use of this model (14) throughout the paper, choosing sufficiently large L_c to eliminate the effects of momentum relaxation at the contacts and allow the bulk properties to be studied.

The qualitative effects of L and L_c can be understood in simple terms by considering the perturbative expression for conductance (6) for a one-dimensional continuum model with tunnelling amplitude $t(x_1, x_2) = t(x)\delta(x_1 - x_2)$, with

$$t(x) = t_0 [\Theta(x) - \Theta(x - L)] * g_{L_c}(x) \quad (15)$$

where the star denotes convolution, and

$$g_{L_c}(x) = \frac{1}{L_c} \frac{2e^{-x/L_c}}{(1 + e^{-x/L_c})^3} \quad (16)$$

For $L \gg L_c$ and $\delta \ll L_c$ this is an accurate approximation to the functional form (14). The matrix element of the tunnel coupling from states k_A to k_B is

$$t_{k_A k_B} \equiv \frac{1}{L_N} \int \int t(x_1, x_2) e^{-ik_B x_1} e^{ik_A x_2} dx_1 dx_2 \quad (17)$$

$$= \frac{t_0}{L_N} \frac{2 \sin\left(\frac{\Delta k}{2} L\right)}{\Delta k} \tilde{g}_{L_c}(\Delta k) \quad (18)$$

where $\Delta k \equiv k_B - k_A$ and

$$\tilde{g}_{L_c}(\Delta k) = \frac{\pi \Delta k L_c (1 + i \Delta k L_c)}{\sinh(\pi \Delta k L_c)} \quad (19)$$

is the Fourier transform of $g_{L_c}(x)$, which was obtained by closing the contour in the correct half-plane and summing the residues of an infinite number of third order poles at $x = (2n + 1)i\pi$. This matrix element enters the perturbative expression for conductance (6) to give

$$G = \frac{2e^2 t_0^2}{\hbar^3 v_A v_B} \frac{\sin\left(\frac{\Delta k}{2} L\right)^2}{(\Delta k)^2} |\tilde{g}_{L_c}(\Delta k)|^2 \quad (20)$$

In the case of momentum conservation, $\Delta k \rightarrow 0$,

$$G = \frac{e^2 t_0^2}{2\hbar^3 v_A v_B} L^2 \quad (21)$$

That is, the conductance grows like the *square* of the tunnelling length L , and is *independent* of the contact length L_c : these results are consistent with the conductance arising from the bulk of the system, unaffected by the contact regions.

For the situation of momentum non-conservation, $\Delta k \neq 0$ the conductance (20) is an oscillatory function of the total length of the system, L . This contribution arises from tunnelling at the contacts, with the oscillatory dependence a consequence of interference between the tunnelling at the contacts at two ends of the sample. Consistent with this explanation, the amplitude of this oscillatory contribution to conductance depends sensitively on the contact lengthscale L_c , with exponential suppression for large $\Delta k L_c$.

B. Rope Geometry

We start by discussing the intertube conductance between the outer shells of two neighbouring nanotubes that lie side by side in a nanotube rope. We choose an

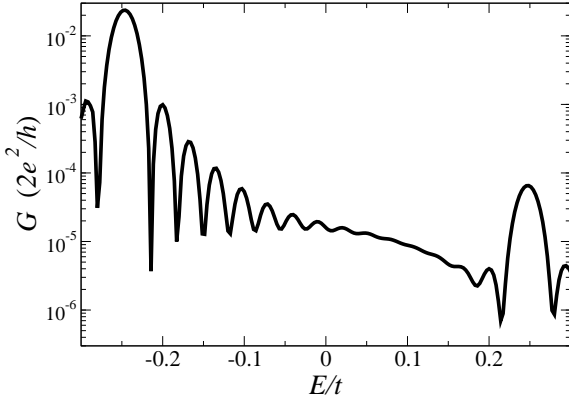


FIG. 4: Intertube conductance between (10, 10) and (18, 0) tubes, in the rope geometry with an intertube distance of $b = 3.4\text{\AA}$. The total length of the carbon nanotubes is $L = 87a$, and intertube tunnelling is introduced smoothly from zero over a length $L_c = 2a$. The peaks at $E/t = \pm 0.25$ correspond to energy-momentum conserving processes described in the text.

intertube separation of $b = 3.4\text{\AA}$ which is typical for a nanotube rope.

If the two tubes are identical, they are commensurate and momentum conservation is satisfied at all energies. We therefore expect strong coupling. Indeed, we find in our numerical calculations (not shown) that for two armchair tubes or two zigzag tubes the intertube conductance is large, reaching of the order of e^2/h even for very short tunnelling regions between the tubes.

Typically, two tubes of different chirality have mismatched Fermi momenta and are incommensurate. As discussed in §IIC, we expect tunnelling to be strongly suppressed. We investigate this effect for the case of (10, 10) armchair and (18, 0) zigzag tubes. In Fig. 4 we show the intertube conductance as a function of the Fermi energy E . (We have suppressed the effects of momentum relaxation at the contacts by choosing $L_c = 2a$.) The conductance is very small for most energies. However, there are two peaks (with sidebands), at $E \approx \pm 0.25t$. At these energies tunnelling can occur by the momentum-conserving tunnelling process discussed at the end of §IIC in which a single reciprocal lattice vector is added to the Fermi momenta of both armchair and zigzag tubes. The presence and positions of these peaks are consistent with the theory of Ref. 5 and formula (8) which showed that the dominant tunnelling processes involve the smallest number of reciprocal lattice vectors. However, the heights are not well reproduced by (8). In particular, the large asymmetry in the conductance at the peaks $E = \pm E_0$, by several orders of magnitude, is not reproduced by Eqn. 8. These failings of Eqn. 8 show that one must go beyond this approximate expression to achieve quantitatively accurate values for the intertube conductance.

The continuum model of §IV A accounts for the qualitative features of the length-dependence of the conduction

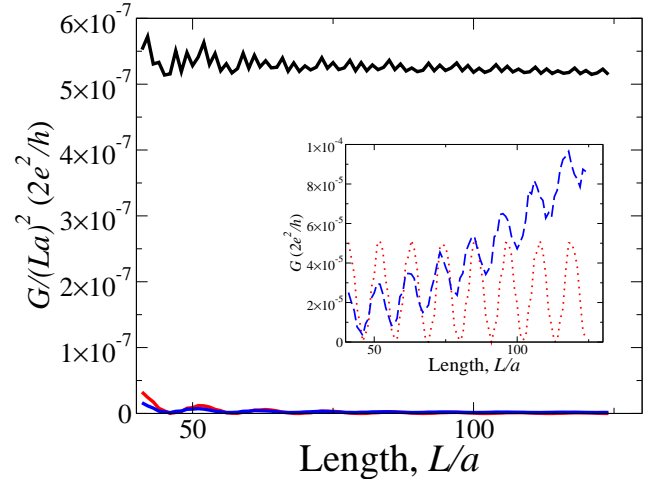


FIG. 5: (Color online) Length dependence of the intertube conductance for (10, 10) and (18, 0) nanotube in a rope geometry a distance $b = 3.4\text{\AA}$ apart. Results are shown as a function of the total length, at $E = -E_0, 0, +E_0$ (solid, dotted, dashed, respectively). The main figure, which plots $G/(La)^2$, indicates clearly that $G \sim L^2$ for $E = E_0$. The inset, which plots G , indicates that $G \sim L^2$ also for $E = -E_0$ but not for $E = 0$. These results are consistent with a momentum conserving tunnelling processes at $E = \pm E_0$ but none at $E = 0$. (A contact length of $L_c = 2a$ has been chosen to minimise effects of momentum relaxation at the contacts.)

tance of the (10, 10) to (18, 0) system. As illustrated in Fig. 5, at $E = \pm 0.25t$ we find that $G \propto L^2$, characteristic of a bulk momentum-conserving tunnelling process [see Eqn. 21]. At $E = 0$ the conductance oscillates with length, indicating that no momentum-conserving processes are contributing. The observed period of the oscillation is consistent with the form $\sin^2(\Delta k L/2)$, with the change in wavevector $|\Delta k| = (2 - \sqrt{3})2\pi/a$ expected from the difference between the Fermi wavevectors of the armchair and zigzag tubes up to a shift by reciprocal lattice vectors.²¹ Furthermore, the contact-induced contribution to the conductance is a strong function of L_c . In Fig. 6 we show this dependence, plotting the conductance at $E = 0$ (averaged over two periods of oscillation) as a function of contact length. As shown in Fig. 6 the rapid decay of conductance with L_c can be fit to the form given by Eqn. 20. Deviations from this form indicate the breakdown of the continuum approximation for small $L_c \lesssim a$.

C. Multiwall Geometry

For the multiwall geometry, in addition to momentum conservation along the tube, the classification of the rotational symmetry, §IID, plays a key role. In order to illustrate this we have calculated the intertube conductance (13) for clean DWNTs of the three different kinds: “zero” (3,3) in (15,0); “intermediate” (5,5) in (18,0); and

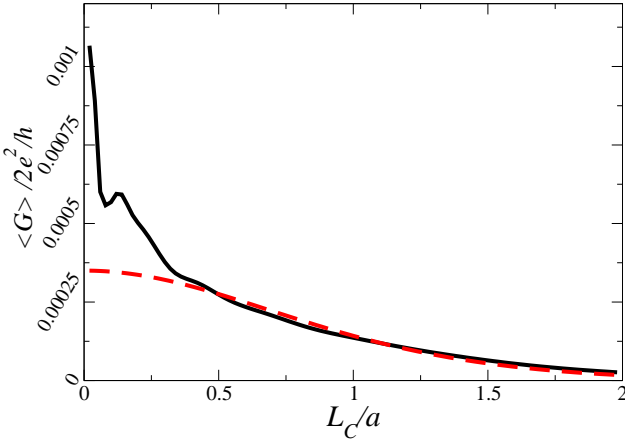


FIG. 6: (Color online) Mean intertube conductance at $E = 0$ between $(10, 10)$ and $(18, 0)$ carbon nanotubes in the rope geometry a distance $b = 3.4\text{\AA}$ apart, as a function of the contact length L_c . The strong dependence on L_c indicates that the conductance is dominated by momentum relaxation at the contacts. The fit (dashed line) is to the functional form of Eqn. 20.

“strong” $(7,7)$ in $(21,0)$. These are chosen to have similar intershell spacing (3.8\AA , 3.7\AA and 3.5\AA respectively). In each case, since the tubes have mismatched Fermi momenta, the conductance is small owing to momentum conservation along the tube. However, the relative sizes of the conductances in these three cases differ greatly: for the “zero” case, we find vanishing intertube conductance to machine accuracy; the conductance of the “strong” coupling case is larger than that of the “intermediate” case by about 8 orders of magnitude (results are not shown here). This very significant difference in conductance indicates the importance of distinction between “strong” and “intermediate” coupling cases.

As in the rope geometry, the conductance is a strong function of the contact length L_c . In Fig.7 this dependence is shown for the average conductance at $E = 0$ of the $(7,7)$ to $(21,0)$ DWNT (which is the “strong” coupling case in terms of the rotational symmetry). Note that, for small values of the contact lengthscale, a conductance of order $0.05e^2/h$ can be induced. This is a sizable conductance, given that it is due only to currents that flow in the vicinity of the contacts. Our results emphasise that to understand the intertube conductance between clean tubes, with mismatched Fermi momenta and incommensurate periodicity, requires a very careful study of the contacts: the conductance is dominated by the current flowing in the vicinity of the contacts.

D. Telescopic Junction

A particularly simple contact geometry between two neighbouring shells of a MWNT or DWNT can be formed by telescopically extension of the inner tubes⁹ and mak-

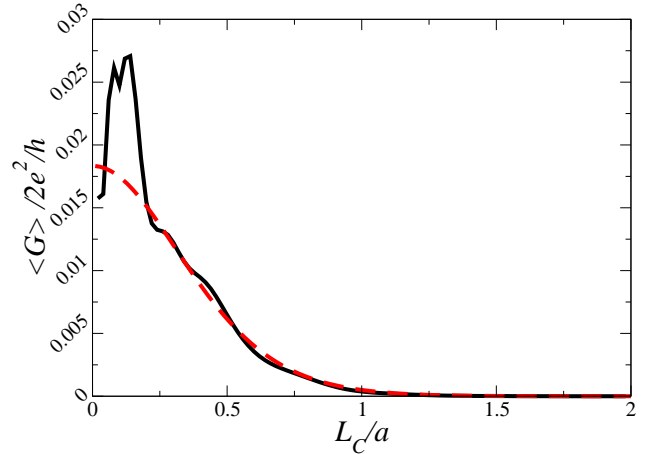


FIG. 7: (Color online) Mean intertube conductance at $E = 0$ between $(7,7)$ and $(21,0)$ carbon nanotubes in a multiwall geometry as a function of the contact length L_c . The strong dependence on L_c indicates that the conductance is dominated by momentum relaxation at the contacts. The fit (dashed line) is to the functional form of Eqn. 20.

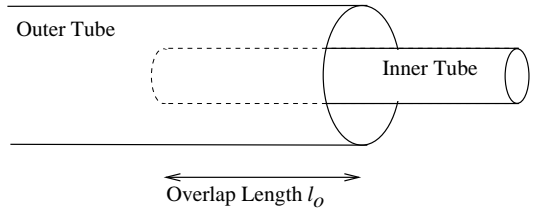


FIG. 8: Schematic picture of a telescopic junction.

ing separate contacts to the inner and outer shells.²² Current that is passed between these two contacts is then forced to flow between the two shells. (See Fig.8.) This geometry involves a very abrupt change in the properties of the tubes at the free ends in the inner and outer tubes. We therefore anticipate that the loss of momentum conservation at the contacts is likely to play a significant role in the intertube conductance.

We have evaluated the conductance for the telescopic junctions formed from clean DWNTs. To model this situation within our approach, the leads $p = 2, 3$ in Fig.2 are disconnected (the τ matrices discussed in §III are set to zero) and the conductance between leads 1 and 4 is calculated. Similar studies have been performed previously for certain commensurate and incommensurate tubes.^{14,23,24,25,26}

Here we focus on the case of incommensurate tubes with mismatched Fermi momenta, and discuss the influence of the rotational symmetry classification of §II D. A telescopic junction does not break the rotational symmetry, so this classification remains relevant. We present results for both “intermediate” [$(10, 10)$ to $(9, 0)$] and “strong” coupling [$(6, 6)$ to $(18, 0)$] in Figs. 9 and 10. (For the “zero” case, we find that the conductance van-

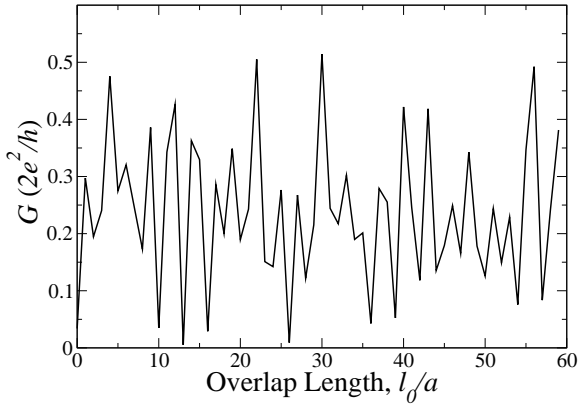


FIG. 9: Conductance of a telescopic junction between two incommensurate (6,6) to (18,0) carbon nanotubes, as a function of the overlap length, ℓ_o . By our classification of the rotational symmetry the coupling is “strong”. The two tubes are strongly coupled even for small overlap lengths.

ishes, as expected by the symmetry analysis.) For the “strong” coupling, Fig. 9, we indeed find very efficient coupling. For even small overlap lengths of a few lattice constants, the conductance is of order e^2/h . Attempting to describe the system as two standing waves in different tubes is no longer valid in this regime: since the intershell conductance is of order e^2/h the tubes are strongly coupled and perturbation theory is inaccurate. For intermediate coupling, Fig. 10, we find an oscillatory intershell conductance but of a very much smaller magnitude. Increasing the overlap does not increase the conductance, consistent with the fact that this is a system with mismatched Fermi momenta, for which there are no bulk momentum-conserving tunnelling processes. These results again highlight the striking difference between rotational symmetry classification as “strong” and “intermediate”. In the former case, the relaxation of momentum at the junction between SWNT and DWNT region is enough to cause a conductance of order e^2/h ; in the latter, the intershell conductance is many orders of magnitude smaller.

V. EFFECTS OF DEFECTS ON INTERTUBE CONDUCTANCE

In §IV the intertube conductance was studied for clean (defect-free) tubes. Momentum conservation was shown to play a very important role in the intertube conductance between tubes with mismatched Fermi momenta. In real samples, electrical conductivity typically depends vitally on the number and type of defects present. One can expect defects to act as scattering centres and to relax momentum conservation. This general point was noted in Ref. 5. However, we are not aware of any studies taking into account the effects of defects on intertube or intershell transport. In this section we provide cal-

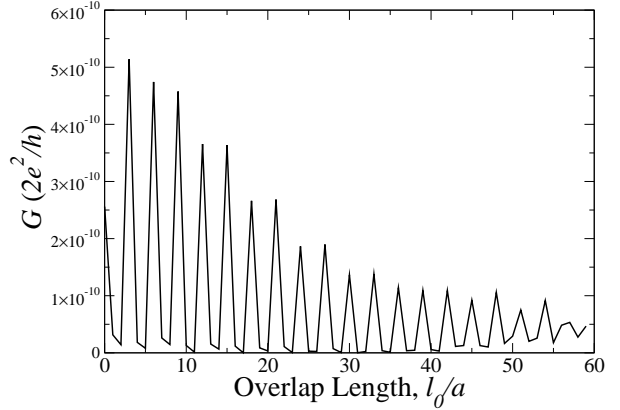


FIG. 10: Conductance of incommensurate (10,10) to (9,0) carbon nanotubes for a telescopic junction, as a function of the overlap length ℓ_o . By our classification of the rotational symmetry the coupling is “intermediate”. The two tubes remain weakly coupled even for large overlap lengths.

culations of the effects of defects of different types on the conductance of incommensurate nanotube ropes and MWNTs. In particular, we discuss the effects of individual scatterers (vacancies and other localised defects) on intertube transport in cases where the clean tubes would have small intertube conductance. We shall then discuss how these results can be extended to a finite density of scatterers.

In all the studies we report below, we use a contact length of $L_c = 2a$ to suppress the effect of momentum relaxation at the contacts and the total length of the central region is made sufficiently long (of order $L = 100a$) that we are able to extract the influence of the impurity in the bulk system without finite size effects.

A. Vacancies

While rare in natively grown nanotubes, vacancies can be introduced by sputtering.⁷ Here we determine the effects of vacancies on intertube conductance in ropes and MWNTs.

1. Rope Geometry

In Fig. 11 we present results for the effects of a vacancy on the conductance between (10,10) and (18,0) carbon nanotubes in the rope geometry. The nanotubes both have diameters of about 1.4nm and are placed 3.4Å apart. The vacancy, which we introduce in the same way as in §III A, is placed on the armchair tube at the point of closest approach.

In Fig. 11 the dashed line shows the intertube conductance for clean tubes, which was discussed in §IV B and shown in Fig. 4 (on a logarithmic scale). With the introduction of a vacancy the conductance around

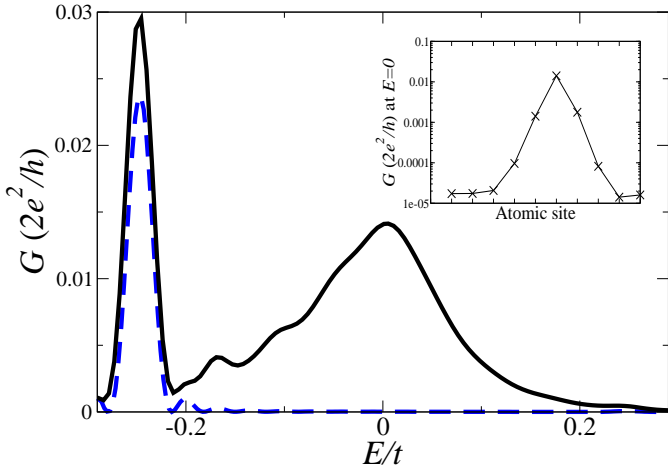


FIG. 11: (Color online) Intertube conductance between a (10, 10) armchair and (18, 0) zigzag in the rope geometry a distance $b = 3.4\text{\AA}$ apart. Results are shown both for clean carbon nanotubes (dashed line) and with a single vacancy placed on a site halfway along the armchair tube (solid line). The inset shows the dependence of the conductance at $E = 0$ on the location of the vacancy at the atomic sites around the circumference of the armchair tube.

$E = 0$ is dramatically increased to a value of order $G \sim 0.01(2e^2/h)$. Note that this is the conductance induced by a *single* vacancy. In a large system containing many such defects one can expect even larger enhancements of the intertube conductance. If the defects contribute incoherently (see Sec. V B 3), the intertube conductance will increase proportionately to the number of defects.

We have investigated the dependence on intertube conductance of the position of the vacancy. (The effect of varying the strength of the potential will be investigated in the next section.) The inset to Fig. 11 plots the results obtained for intertube conductance at $E = 0$ by moving the vacancy around the circumference of the tube on the 10 sites of the (10, 10) armchair tube that are crystallographically equivalent. The position of the vacancy has significant impact on the intertube conductance, with the largest enhancement of intertube conductance when the vacancy site is closest to the other nanotube. This indicates that the wave that is backscattered by the vacancy in the defective tube has a large amplitude localised in the vicinity of the vacancy.

An experimental investigation of the effects of vacancies (introduced intentionally by sputtering) on the conductance of nanotube ropes was carried out by Stahl *et al.*⁷ The results were interpreted in terms of the intertube tunnelling between metallic tubes of *matching* chirality in a rope consisting of a random distribution of tubes of random chiralities. Tunnelling between carbon nanotubes of different chiralities was ignored in the analysis, based on the existing theory⁵ for clean tubes which showed that this tunnelling is heavily suppressed as a result of momentum conservation. Our results show

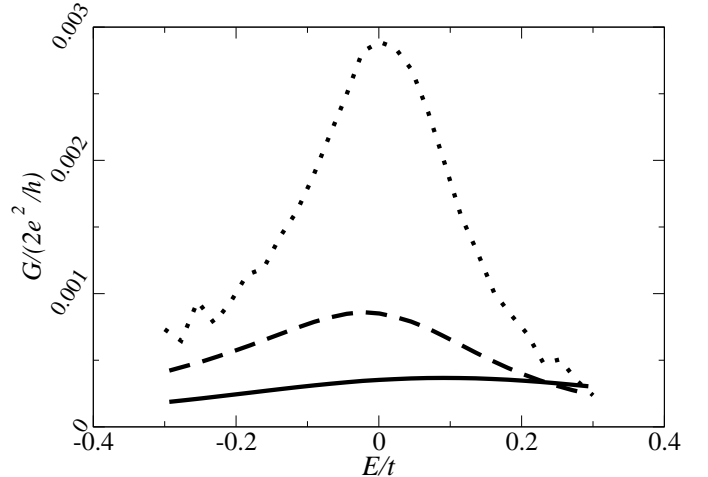


FIG. 12: Intershell conductances for DWNTs in the presence of a single vacancy (placed on the inner tube), for the three types of coupling determined by the angular symmetry of §IID. The solid line is a (3, 3) to (15, 0) system (“zero” coupling); the dashed line is a (5, 5) to (18, 0) system (“intermediate” coupling); and the dotted line is a (7, 7) to (21, 0) (“strong” coupling).

that, owing to the loss of momentum conservation in the vicinity of the vacancy, the intertube transport between nearest neighbour tubes of *different* chirality can occur efficiently. Even for a single vacancy, the intertube conductance between two neighbouring tubes can be as large as $0.01(2e^2/h)$, corresponding to a resistance of around $1\text{M}\Omega$. This is well within the range of intertube resistances that was measured in Ref. 7. Our results therefore indicate that owing to the loss of momentum conservation at the vacancies, the tunnelling between incommensurate certainly carbon nanotubes cannot be neglected in these experiments, and is likely to play a significant role.

2. Multiwall Geometry

We now consider the effects of a vacancy in a DWNT geometry. The vacancy breaks the rotational symmetry described in §IID thereby removing the distinction between the different strengths of coupling of the metallic subbands. Therefore, if all other parameters are equal, one would expect the differences between “Zero”, “Intermediate” and “Strong” cases to disappear. Fig. 12 shows the conductance for the same three DWNTs considered in §IV C, now with a single vacancy in the armchair tube. The magnitude of the intertube conductance for all three types is now $G \approx 10^{-3} (2e^2/h)$ around $E = 0$. Recalling that the intertube conductances for clean tubes, discussed in §IV C, differ by many orders of magnitude in these three cases, one indeed see that the vacancy does break the distinction between these cases giving conductances of similar magnitudes. Furthermore, the overall size of the conductance is very much increased. Again,

the presence of even a single vacancy can very significantly affect the conductance between the shells of a MWNT.

B. Other Types of Defect

The nature of the dominant defect scattering in high quality nanotubes is not well characterised. Indeed, it is likely to vary between systems involving different preparation methods and different geometries. The disparity between the intershell MWNT conductance experiments of vertically suspended MWNTs²⁸ and those where the MWNTs are placed on a substrate⁸ suggests that defects may arise due to substrate effects. We have studied the effects of various types of localised defects, including potential defects and deformations of the outer tube arising from substrate roughness.

We focus on the case of MWNTs, in order to make connection with the experimental measurements of Bourlon *et al.*⁸ We have calculated the effects on the conductance at $E = 0$ of a single defect in the outer shell of a DWNT, consisting of a (13, 13) armchair (outer shell) and a (12, 0) zigzag (inner shell) carbon nanotube. According to our classification of rotational symmetry, this combination is of “intermediate” coupling, which is the typical case. The effect of a single defect is determined by choosing a sufficiently long section of tube L and sufficiently smooth contacts L_c that finite size effects are negligible. In order to quantify the effect of the scattering, we report dimensionless measures of intratube resistance, and intertube conductance, defining the quantities

$$R_s \equiv 1 - \frac{T_s}{2} = 1 - \frac{1}{2} \sum_{\mu, \mu'} T_{\mu, 1; \mu', 2} \quad (22)$$

$$I_s \equiv \sum_{\mu, \mu'; p=1, 2; p'=3, 4} T_{\mu, p; \mu', p'} \quad (23)$$

R_s is a measure of the intratube backscattering,³¹ and I_s is a measure of the intertube conductance. In §VB3 we shall discuss how these quantities can be used to compare with experiment.⁸

1. Potential Scatterer

We consider a potential centred on a site \mathbf{r}_0 of the outer carbon nanotube with strength V_0 and correlation length, ξ , such that there is an additional site potential on this tube of

$$V_i = V_0 e^{-|\mathbf{r}_i - \mathbf{r}_0|^2 / \xi^2} \quad (24)$$

This is a model for several types of defect: molecules absorbed onto the surface of the MWNT; a residual potential due to the close proximity to the substrate; nitrogen substitution, which can be modelled by choosing $V_0 \approx -2.5$ eV.²⁹

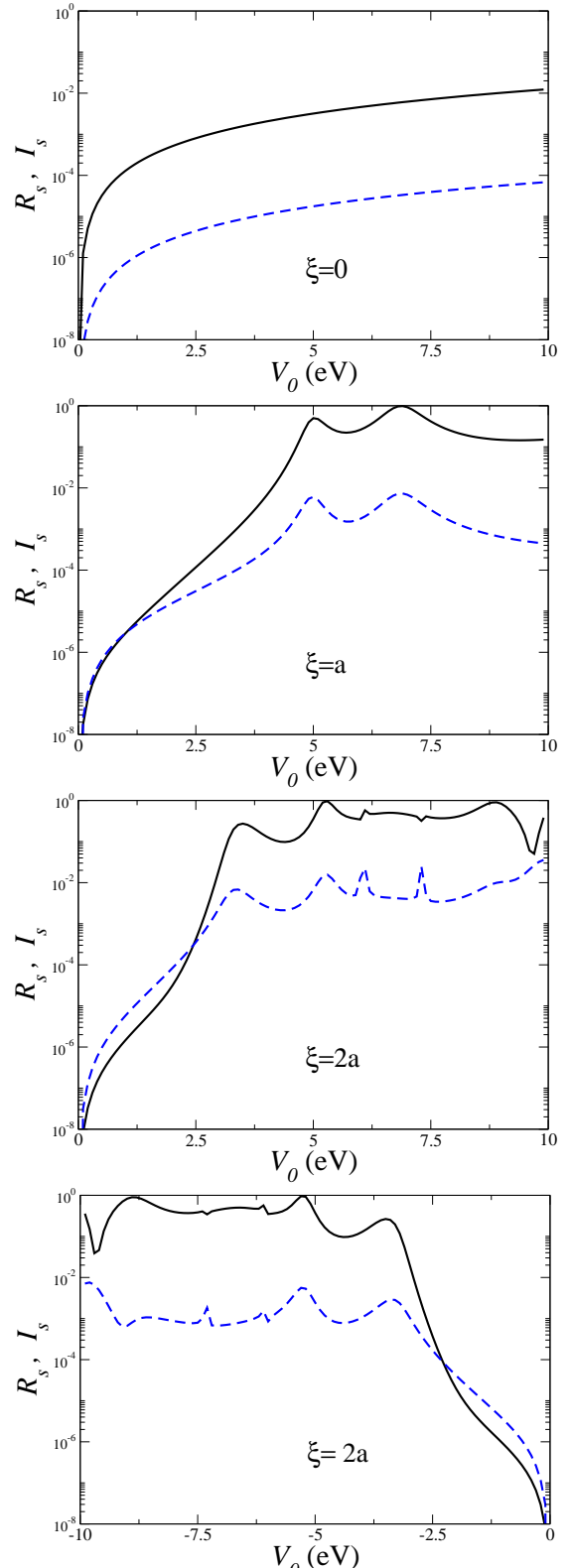


FIG. 13: (Color online) The dimensionless measures of backscattering, R_s , (solid line) and intertube scattering, I_s , (dashed line) for a (13,13) to (12,0) DWNT with a single potential defect, of varying strengths V_0 and correlation length ξ [see Eqn. 24]. The total length of the system is $L = 87a$ with tunnelling introduced smoothly via a contact length of $L_c = 2a$, so boundary effects are minimal and the results are characteristic of a single defect in the bulk.

In Fig. 13 the dimensionless parameters of Eqns. 22 and 23 are plotted against potential strength V_0 for different values of the correlation length, ξ . In each case, the backscattering R_s and intertube coupling I_s increase at small V_0 as V_0^2 consistent with expectations from perturbation theory. In this weak scattering regime, the relative sizes of the backscattering and intertube scattering depend strongly on the correlation length ξ . One might expect that increasing the range of the potential ξ at fixed amplitude V_0 would cause a larger effect of the defect as the total integrated weight of the potential increases. This is true for I_s and for R_s at large V_0 . However, for small V_0 , the intratube backscattering R_s actually falls with increasing ξ , even to below I_s for $\xi = 2.0a$: in this case, the defect more efficiently causes intertube scattering than it does intratube backscattering. This strong dependence on the correlation length can be understood as a consequence of the suppression of intratube backscattering due to the conservation of “pseudo-spin” by the (perturbative) scattering from a potential with range larger than a lattice constant.^{2,3,4} For large ξ the backscattering parameter R_s becomes small; there is no such suppression of intertube scattering, so I_s remains large.

The effects of the potential scatterer are very similar for both positive and negative V_0 . For $\xi = 0$, both R_s and I_s are symmetric in V_0 . For $\xi \neq 0$, an asymmetry in V_0 arises, but, as shown in Fig. 13, even for $\xi = 2a$ the asymmetry remains very small.

2. “Dent” Scatterer

One possible source of scattering in the measurements of Bourlon *et al.*⁸ is the roughness of the substrate, which could lead to deformation of the MWNT.⁸ We investigate this by considering a “dent” in the outer shell, which when placed at a position \mathbf{r}_0 gives rise to a correlated displacement of the atoms. We displace the atom i (with undeformed position \mathbf{r}_i) in the radial direction towards the tube axis by a distance

$$\delta r_i = d_0 e^{-|\mathbf{r}_i - \mathbf{r}_0|^2/\xi^2}. \quad (25)$$

These displacements will change the inter- and intra-tube hopping parameters and could also lead to additional on-site potentials. Provided the curvature of the tube is negligible, the correction to the intratube hopping and onsite potential is of order $(d_0/a)^2$ (by symmetry there can be no term linear in d_0). However, the correction to the intertube hopping is of order d_0/a . We therefore consider only the changes to the intertube hopping, which is accurate for small deformations $d_0 \ll a$.

Fig. 14 shows the results of calculations of R_s and I_s , Eqns. 22 and 23, for a single potential defect of various correlation lengths ξ as a function of the strength V_0 . Compared to the potential scatterers, the “dent” scatterers give qualitatively different results. Now, the intertube

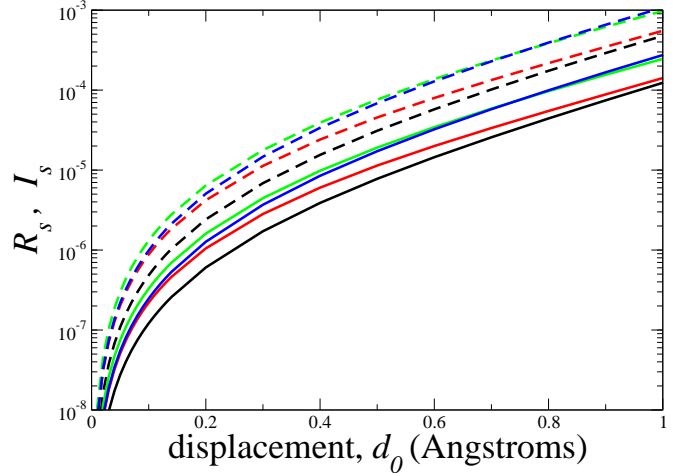


FIG. 14: (Color online) The dimensionless measures of backscattering, R_s , (solid lines) and intertube scattering, I_s , (dashed lines) for a (13,13) to (12,0) DWNT with a single “dent” in the outer shell as a function of the displacement d_0 and correlation length ξ [see Eqn. 25]. Results are shown for the set of correlation lengths $\xi = 0.00, 1.76, 3.53, 5.29\text{\AA}$, which may be assigned to the graphs by noting that both R_s and I_s increase with increasing ξ for $d_0 \sim 1\text{\AA}$.

conductivity is always higher than the intratube resistivity. This is a consequence of the displacement having no effect on the intratube tight-binding parameters (valid for $d_0 \ll a$): intratube backscattering involves a second order process in which the electron tunnels to and from the other tube. Thus our results indicate that the dent scatterer especially enhances the intertube conductance as compared to the intratube resistance.

3. Experimental Comparison

In the experimental studies of Bourlon *et al.*⁸, non-local voltages induced between contacts to the outer shell of MWNTs were used to extract the intrashell resistivity, $\rho_{\text{intra}}^{\text{exp}} = (6 - 25)\text{k}\Omega\mu\text{m}^{-1}$, for each of the outer two shells and an intershell conductivity, $g_{\text{inter}}^{\text{exp}} = [(3.7 - 20)\text{k}\Omega]^{-1}\mu\text{m}^{-1}$, between these two outer shells. (Contributions from other shells were shown to be small.) As emphasised in Ref. 8, the intertube conductivity cannot be understood within existing theoretical descriptions of intershell coupling in incommensurate nanotubes. We believe, as suggested in Ref. 8, that the discrepancy is due to the effects of disorder which was not considered in previous theoretical works. We can use our results on impurity scattering to estimate the intrashell resistivity and intershell conductivity in the experiments. Since the nature and density of defects are very uncertain in these experimental systems, our approach is to search for parameter regimes that are consistent with the experimental results. This provides constraints on the nature

of the defects in these systems.

Comparing the results of our calculations with these experimental results⁸ requires a number of simplifying assumptions.

While the MWNTs used in the experiments contained around 20 shells, since transport was shown to be largely confined to the outer two shells we consider just two coaxial shells. We use the results shown above on the (13, 13) to (10, 0) system, which is a large radius system showing the effects of incommensurability, and with typical “intermediate” coupling. The overall diameter of this system, of about $d = 16\text{\AA}$, is much smaller than the diameter $D = 17\text{nm}$ of the outer shell of the MWNTs in the experiment. We take account of this difference by scaling the scattering rates we obtain in the numerics on a system with diameter d by a factor of $(d/D)^2 \sim 1/100$.³⁰ [This reduction reflects the reduction in the matrix element of a localised potential as $1/D$, and thus a reduction in scattering rate (using Fermi’s golden rule) as $1/D^2$.]

In the experimental system the tubes are doped such that several modes are occupied, with the estimated number of modes $N_m = 10 - 20$.⁸ There are then $2N_m$ Fermi points in each shell. Generically, the Fermi momenta of adjacent shells will not coincide and the shells will be incommensurate. We take the results of the above calculation of the effects of defects on the transport between the metallic bands of armchair and zigzag tubes as a measure of the scattering probabilities between states at the individual Fermi points of the two outer shells of the MWNTs in Ref. 8. We consider the limit of weak backscattering and weak intershell scattering from a single defect. In our numerical results, each shell has 4 Fermi points, and we use the total intertube scattering probability I_s to obtain the intertube scattering probability between individual Fermi points as $I_s/4^2$ (assuming that the 4 Fermi points in one tube scatter equally to the 4 Fermi points in the other). Then, for N_m modes, we extend to $2N_m$ Fermi points in total to obtain that the scattering probability for a single incoming mode into any of the modes on the second tube is

$$p_I = (2N_m) \frac{I_s}{4^2} \left(\frac{d}{D} \right)^2 \quad (26)$$

which incorporates the reduction of $(d/D)^2$ discussed above. Similarly for the reflection probability, extending from the case (in the numerics) of two backscattering modes to N_m backscattering modes, the mean backscattering probability for a single incoming mode into any of the modes on the second tube is

$$p_R = (N_m) \frac{R_s}{2} \left(\frac{d}{D} \right)^2. \quad (27)$$

We have ignored current conservation in these estimates, which would involve the introduction of compensation between intertube and backscattering probabilities; this assumption is valid provided scattering is weak, and both p_I and p_R are small.

The experiments involve the scattering by many defects, while the above numerical results are for a single scatterer. We extend to larger numbers of scatterers by assuming that the scatterers combine *incoherently*, with n_s defects per unit length. This will give a good approximation to the transport properties provided the system is not in a strongly localised regime. The experimental samples are far from the strongly localised regime even down to low temperatures: from the experimental measurements the conductance on the lengthscale of the contact separation ($\lesssim 1\mu\text{m}$) remains large compared to e^2/h .

Within these assumptions, and using the analysis presented in Appendix IX we find that, for n_s scatterers per unit length, the intertube conductivity g_{inter} and intratube resistivity ρ_{intra} (both per unit length) are

$$g_{\text{inter}} \equiv \frac{G_{\text{inter}}}{L} = \left(\frac{2e^2}{h} \right) \frac{I_s N_m^2}{4} n_s \left(\frac{d}{D} \right)^2 \quad (28)$$

$$\rho_{\text{intra}} \equiv \frac{R_{\text{intra}}}{L} = \left(\frac{h}{2e^2} \right) \frac{R_s}{2} n_s \left(\frac{d}{D} \right)^2 \quad (29)$$

Note that, within this weak scattering approximation, the resistivity is independent of the number of modes: as N_m increases, the increased number of Fermi points into which backscattering can occur (increasing the resistivity) is compensated by the increase in the number of modes available for conduction (increasing the conductance). On the other hand the intertube conductance increases as the *square* of the number of modes, N_m : one factor coming from the number of incoming modes, and one factor from the increased number of Fermi points into which any one mode can be scattered in the other shell.

We are now in a position to compare our results with the experimental results.⁸ It is helpful to note that within our theory the ratio of g_{inter} to ρ_{intra} is independent of the defect density

$$\frac{g_{\text{inter}}}{\rho_{\text{intra}}} = \left(\frac{2e^2}{h} \right)^2 \frac{N_m^2}{2} \frac{I_s}{R_s} \quad (30)$$

In the experiments,⁸ this ratio is of order $g_{\text{inter}}^{\text{exp}}/\rho_{\text{intra}}^{\text{exp}} \sim (2e^2/h)^2$. Agreement of the theory (30) with this experimental value requires $R_s/I_s \sim 0.5N_m^2 \sim (50 - 200)$, using the estimate⁸ $N_m \sim 10 - 20$. Within the wide range of uncertainty in the parameters, the experimental results are consistent with our results for potential defects with vanishing correlation length $\xi = 0$, for which we find $R_s/I_s \simeq 180$ over the range of V_0 shown in Fig.13(a), or for potentials with a small correlation length. In our calculations, the ratio R_s/I_s becomes small for potential scatterers with large correlation lengths; this reduction is likely to be overestimated in a calculation based on metallic bands alone. Note that in the case of “dent” defects we find that $R_s/I_s \ll 1$ in all cases (Fig.14). Thus, our analysis shows that the experimental results are consistent with the dominant disorder being potential scatterers with a small correlation length, but are *not*

consistent with the dominant disorder being “dents” in the outer tube caused by substrate roughness.³²

To estimate the strength of the disorder, we focus on the case of potential defects with vanishing correlation length, $\xi = 0$. From the results in Fig.13(a), we find that $R_s \sim 1.3 \times 10^{-4} (V_0/\text{eV})^2$ over the range of V_0 shown. Matching (29) to $\rho_{\text{intra}}^{\text{exp}} \sim 10 \text{k}\Omega\mu\text{m}^{-1}$ sets an estimate for the required number of potential scatterers n_s per unit length as a function of their strength V_0 . Converting to the number of scatterers per atom, $\sqrt{3}a^2 n_s/(4\pi D)$, we find agreement for a root mean square potential energy fluctuation on each site of about 0.8eV. This is comparable to the disorder strengths required by other theoretical studies to account for a resistivity of this size. [Indeed, Eqn. 29 closely matches the results of Ref. 30, for $N_m = 2$, relating mean-free-path to resistivity by the Drude formula.]

In summary, our theory shows that the dramatic increase of intershell coupling arising from scattering from disorder is sufficient to account for the experimental observations. We find quantitative agreement (within the uncertainties of the experimental parameters) for a model of disorder consisting of short-range potential scatterers. We note that our theory shows that the relative sizes of the intershell scattering and intrashell backscattering depend strongly on the number of modes N_m , with $g_{\text{inter}}/\rho_{\text{intra}} \propto N_m^2$. It would be interesting to test this prediction in experiment.

VI. CONCLUSIONS

We have studied the transport between aligned carbon nanotubes (or nanotube shells) in both rope and multiwall geometries. We focused on cases of two metallic nanotubes of different chiralities, with mismatched Fermi momenta and incommensurate periodicities. Our numerical calculations show clear evidence of the importance of momentum conservation, and of a classification we introduced for the rotational symmetry of a pair of shells in a MWNT. For clean tubes, we find that the loss of momentum conservation at the contacts dominates the intertube transport.

We studied in detail the effects of localised defects on the intertube transport in incommensurate nanotube ropes and MWNTs. Defects break momentum conservation, and the rotational symmetry in multiwall geometries. We find that the intertube conductance of incommensurate nanotubes is very dramatically increased by even a single vacancy. Our results show that the introduction of vacancies to nanotube ropes enhances the tunnelling between incommensurate tubes sufficiently to make this defect-mediated tunnelling a dominant transport mechanism.⁷ We calculated the effects of localised defects of various types on the intra- and inter-shell transport of MWNTs. For a potential scatterer, we find a strong dependence on the range, ξ , of the potential: for large ξ , intratube backscattering is suppressed^{2,3,4} but in-

tertube scattering remains large. For a “dent” scatterer, involving a localised depression of the outer shell, intertube conductance is very much enhanced with intratube backscattering remaining small.

Our results establish the extreme sensitivity to disorder of the intertube transport of incommensurate nanotubes with mismatched Fermi momenta. They provide the first calculations of the quantitative effects of this scattering on the transport between nanotube shells in rope and multiwall geometries. A comparison of the results of our calculations with experimental measurements⁸ shows agreement with our theory for a model of disorder consisting of short-range potential scatterers. Potential scatterers with large correlation lengths and deformations of the outer shell are not consistent with the experimental results.

Finally, we would like to comment briefly on the effects of electron-electron interactions. In a one-dimensional metal, interactions lead to a smearing of the Fermi surface, so that there is no longer a discontinuity in the occupation numbers at the Fermi surface.³⁴ Owing to the central role played by momentum conservation in our considerations, it is important to ask whether this smearing of the Fermi surface could affect our results. We find that including interactions within a Luttinger liquid analysis does not change the essential behaviour described above for non-interacting electrons:³⁵ the intertube conductance is still strongly suppressed for incommensurate nanotubes with mismatched Fermi wavevectors, and is strongly enhanced by impurity scattering. The interactions will, in addition, cause the overall intertube conductance to be suppressed as a power law in temperature (or bias), as is familiar from tunnelling into a Luttinger liquid. These interaction effects will be weaker at high temperatures and for MWNTs with many occupied subbands.³⁶

Acknowledgments

We are grateful to Dr R. Roemer and Prof. M. Payne for helpful comments. This work was supported by the EPSRC Grant GR/R99027/01.

VII. GREEN’S FUNCTIONS FOR SEMI-INFINITE NANOTUBES

To determine the Green’s functions we make use of the form

$$\langle i, \alpha | G | j, \beta \rangle = \sum_{\mu, k} \frac{\langle i, \alpha | \Psi_{\mu, k} \rangle \langle \Psi_{\mu, k} | j, \beta \rangle}{E - \epsilon_{\mu, k} + i\delta}, \quad (31)$$

where $|\Psi_{\mu, k}\rangle$ are energy eigenstates, μ is the mode index and k is the wavevector along the axis of the carbon nanotube. Positions are labelled by i, α , with i labelling the 1D unit cell (along the tube axis), and α the atoms within this 1D cell.

A. Armchair Tube

The metallic bands in an armchair carbon nanotube have energy dispersion relations

$$\epsilon_{\mu=\pm,k} = \mp t \left[1 - 2 \cos \left(\frac{ka}{2} \right) \right] \quad (32)$$

where $\mu = \pm$ labels the two metallic bands, k is wavevector along the axis of the nanotube. For a tube with periodic boundary conditions, we write the wavefunction $|\Psi_{\mu,k}\rangle$ in the form

$$\langle i, \alpha | \Psi_{\mu,k} \rangle = \frac{e^{ikx_i}}{\sqrt{\frac{N_{1D}}{2}}} \chi_{\mu,k}(\alpha) \quad (33)$$

where x_i is the distance of the 1D unit cell along the tube axis, N_{1D} is the number of 1D unit cells. The functions $\chi_{\mu,k}$ are easily obtained from the free-particle eigenstates; explicitly for an (n,n) tube they are

$$\chi_{\pm,k}(\alpha) = \frac{1}{\sqrt{4n}} \begin{pmatrix} 1 \\ \pm e^{ik\frac{ka}{2}} \\ -e^{ik\frac{ka}{2}} \\ \mp 1 \\ \vdots \end{pmatrix} \quad (34)$$

$$\langle i, \alpha | G | j, \beta \rangle = \frac{1}{8\pi n} \sum_{\mu} \int_{-2\pi}^{2\pi} d(ka) \frac{e^{iak(i-j)} \chi_{\mu,k}(\alpha) \chi_{\mu,k}^*(\beta)}{E - \epsilon_{\mu,k} + i\delta} - \frac{e^{iak(i+j-1)} \chi_{\mu,k}(\alpha) \chi_{\mu,k}(\beta)}{E - \epsilon_{\mu,k} + i\delta} \quad (36)$$

The calculation simplifies further by considering only the Green's function at the end of the carbon nanotube, i.e. $i = j = 1$. (This is all that is required in our calculations of the influence of the semi-infinite leads in §III.) The dependency on the inner product in Eqn. 36 (describing the coupling between the different sites labelled by α) can be reduced to a 2×2 matrix, since there are only two types of atom on the “edge” of the armchair nanotube. Using contour integration in the variable $z = e^{\pm i\frac{ka}{2}}$, we find the Green's function for an armchair carbon nanotube³³

$$\langle \alpha | G | \beta \rangle = \frac{1}{2nt} \begin{pmatrix} -z_+ + z_- & z_+ + z_- \\ z_+ + z_- & -z_+ + z_- \end{pmatrix} \quad (37)$$

where

$$z_{\pm} \equiv \left(\frac{1 \mp E/t}{2} \right) \pm i \sqrt{1 - \left(\frac{1 \mp E/t}{2} \right)^2} \quad (38)$$

B. Zigzag Green's Functions

The two metallic bands in an $(n,0)$ zigzag tube have modes, μ , which are distinguished by the subband indices

where the atoms in the 1D unit cell are labelled in order of their angular positions around the tube.

For a finite length tube, the wavefunction is a standing wave, chosen to satisfy the boundary conditions at the two ends of the carbon nanotube, which places restrictions on the allowed values of k . The armchair finite tube wavefunctions take the form

$$\langle i, \alpha | \Psi_{\mu,k} \rangle = \frac{e^{ik\frac{ka}{2}}}{C} \left[e^{-i\frac{ka}{2}} e^{ikx_i} \chi_{\mu,k}(\alpha) - e^{i\frac{ka}{2}} e^{-ikx_i} \chi_{\mu,k}^*(\alpha) \right] \quad (35)$$

where $C = \sqrt{8nN}$ is a normalisation factor, which is independent of k for a long tube.

Substituting the wavefunctions and energy dispersion relation into Eqn. 31 we can convert the summation to an integral, and using symmetry relations and the fact that the resultant integral is analytic at $k = 0$ we find

$q_{\mu} = 2n/3, 4n/3$. They are degenerate with energies

$$\epsilon_{\mu,k} = \pm 2t \sin \left(\frac{\sqrt{3}ka}{4} \right) \quad (39)$$

for the right and left moving modes (\pm). For a tube of finite length, the boundaries induce reflections but no mixing between the bands of different q since rotational symmetry is preserved. The finite tube wavefunctions take the form

$$\langle i, \alpha | \Psi_{\mu,k} \rangle = \frac{e^{iq_{\mu} \frac{2\pi}{n} y_{\alpha}}}{C} \left[e^{ikx_i} \chi_{\mu,k}(\alpha) - e^{-ikx_i} \chi_{\mu,-k}(\alpha) \right] \quad (40)$$

with the same notation as in the armchair case (but note that the 1D unit cell and associated wavefunctions χ are now those appropriate for the zigzag tube).

We proceed as in the armchair case by restricting our attention to the relevant atoms on one end of the carbon nanotube. Converting the summation to an integral and using residue calculus we find the total metallic Green's function on the end of a semif-infinite zigzag carbon nanotube to be

$$\langle \alpha | G | \beta \rangle = \frac{2}{nt} e^{i \frac{2\pi}{3a} (y_\alpha - y_\beta)} \left(1 + e^{i \frac{2\pi}{3a} (y_\alpha - y_\beta)} \right) \left[\frac{E}{2t} - i \sqrt{1 - \left(\frac{E}{2t} \right)^2} \right] \quad (41)$$

where the terms of two periodicities in $y_\alpha - y_\beta$ arise from the $4n/3$ and $2n/3$ bands.

VIII. TRANSMISSION PROBABILITIES

Here we state the transmission probabilities across a scattering region between armchair and zigzag carbon

nanotubes. Following §III the input wave is labelled by mode μ and lead p , and the output by mode μ' and lead p' . One must distinguish between the cases where the input and output leads are of the differing chiralities.

$$p \text{ armchair, } p' \text{ armchair} \quad T_{\mu,p;\mu',p'} = \left| -\delta_{p,p'} \delta_{\mu,\mu'} + 2 \frac{\hbar}{at} v_{ac} \langle \chi_\mu | \mathcal{G} | \chi_{\mu'} \rangle \right|^2 \quad (42)$$

$$p \text{ zigzag, } p' \text{ zigzag} \quad T_{\mu,p;\mu',p'} = \left| -\delta_{p,p'} \delta_{\mu,\mu'} + 2 \frac{2\hbar}{\sqrt{3}at} v_{zz} \langle \chi_\mu | \mathcal{G} | \chi_{\mu'} \rangle \right|^2 \quad (43)$$

$$p \text{ armchair, } p' \text{ zigzag (or vice versa)} \quad T_{\mu,p;\mu',p'} = \left| \frac{2\hbar}{at} \sqrt{\frac{2}{\sqrt{3}}} v_{zz} v_{ac} \langle \chi_\mu | \mathcal{G} | \chi_{\mu'} \rangle \right|^2 \quad (44)$$

We use the terminology and definitions for the carbon nanotube wavefunctions described in Appendix VII, and v_{ac} and v_{zz} are the velocities for armchair and zigzag tubes. The inner product of the Green's function with the 1D wavefunctions $\chi_\mu \chi_{\mu'}$ are to be taken on any 1D unit cell in the leads p and p' (wavevector labels are suppressed, but should be understood to be the Fermi wavevectors of the leads). The Kronecker delta functions represent the modification required for reflection back into the same lead and mode.

IX. INCOHERENT SCATTERING SUMMATION

We illustrate the method used to combine probability s -matrices, which enables us to calculate conductance through many scattering centres incoherently, as used in §VB3. Consider the setup in Fig. 15. For two identical scattering sections we have

$$\begin{pmatrix} L_{\text{out}} \\ M_{\text{out}} \end{pmatrix} = \begin{pmatrix} \mathbf{R} & \mathbf{T} \\ \mathbf{T} & \mathbf{R} \end{pmatrix} \begin{pmatrix} L_{\text{in}} \\ M_{\text{in}} \end{pmatrix} \quad (45)$$

$$\begin{pmatrix} M_{\text{in}} \\ R_{\text{out}} \end{pmatrix} = \begin{pmatrix} \mathbf{R} & \mathbf{T} \\ \mathbf{T} & \mathbf{R} \end{pmatrix} \begin{pmatrix} M_{\text{out}} \\ R_{\text{in}} \end{pmatrix} \quad (46)$$

where L_{out} is a vector representing the probability flux of all the outgoing modes to the left of the scatterer, and

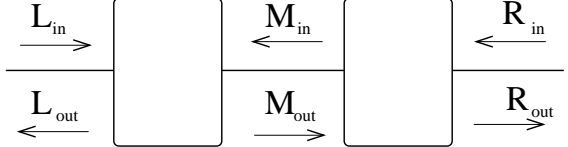


FIG. 15: Combining two identical scattering sections

L_{in} is a vector representing the probability flux of all the ingoing modes to the left, similarly for M and R . \mathbf{R} and \mathbf{T} are matrices representing the reflection and transmission of different leads. We assume that the scattering sections are symmetric in space. We can eliminate the M terms to obtain the combined structure

$$\begin{pmatrix} L_{\text{out}} \\ R_{\text{out}} \end{pmatrix} = \begin{pmatrix} \mathbf{R}' & \mathbf{T}' \\ \mathbf{T}' & \mathbf{R}' \end{pmatrix} \begin{pmatrix} L_{\text{in}} \\ R_{\text{in}} \end{pmatrix} \quad (47)$$

where

$$\mathbf{T}' = \mathbf{T} [\mathbf{I} - \mathbf{R}^2]^{-1} \mathbf{T} \quad (48)$$

$$\mathbf{R}' = \mathbf{R} + \mathbf{T} \mathbf{R} [\mathbf{I} - \mathbf{R}^2]^{-1} \mathbf{T} \quad (49)$$

For the setup with two carbon nanotubes, it is useful to separate tubes A and B:

$$\begin{pmatrix} L_{\text{out}}^A \\ R_{\text{out}}^A \\ L_{\text{out}}^B \\ R_{\text{out}}^B \end{pmatrix} = \begin{pmatrix} \mathbf{R}^A & \mathbf{T}^A & \mathbf{I} & \mathbf{I} \\ \mathbf{T}^A & \mathbf{R}^A & \mathbf{I} & \mathbf{I} \\ \mathbf{I} & \mathbf{I} & \mathbf{R}^B & \mathbf{T}^B \\ \mathbf{I} & \mathbf{I} & \mathbf{T}^B & \mathbf{R}^B \end{pmatrix} \begin{pmatrix} L_{\text{in}}^A \\ R_{\text{in}}^A \\ L_{\text{in}}^B \\ R_{\text{in}}^B \end{pmatrix} \quad (50)$$

where \mathbf{I} is the intertube transmission probability, which has been set equal between all modes to simplify the problem. Taking one mode per tube, adding N_s identical scatterers, and expanding in a power series in terms of I , the intertube transmission probability, the leading behaviour of the relevant probabilities is

$$T_{N_s} = \frac{T}{N_s - (N_s - 1)T} \quad \lim_{N_s \rightarrow \infty} \rightarrow \frac{T}{N_s(1 - T)} \quad (51)$$

$$I_{N_s} = N_s I \quad (52)$$

where T_{N_s} is the total intratube transmission probability through N_s scatters if T is the probability of transmission through one scatterer, and I_{N_s} is the total intertube transmission probability through N_s scatterers if I is the probability of transmission through one scatterer. We make use of these results in §VB3, in the limit of weak scattering $1 - T, I \ll 1$.

¹ R. Saito, *Physical Properties of Carbon Nanotubes*, 1 ed. (Imperial College Press, 1998).

² T. Ando and Nakanishi, J. Phys. Soc. Japan **67**, 1704 (1998).

³ T. Ando, T. Nakanishi, and R. Saito, J. Phys. Soc. Japan **67**, 2857 (1998).

⁴ P. L. McEuen, M. Bockrath, D. H. Cobden, Y.-G. Yoon and S. G. Louie, Phys. Rev. Lett. **83**, 5098 (1998).

⁵ A. Maarouf, C. L. Kane, and E. J. Mele, Phys. Rev. B **61**, 11156 (2000).

⁶ Y. Yoon and S. G. Louie, Phys. Rev. B **66**, 073407 1 (2002).

⁷ H. Stahl, J. Appenzeller, R. Martel, Ph. Avouris, and B. Lengeler, Phys. Rev. Lett. **85**, 5186 (2000).

⁸ B. Bourlon, C. Miko, L. Forró, D. C. Glattli, and A. Bachtold, Phys. Rev. Lett. **93**, 176806 (2004).

⁹ J. Cumings and A. Zettl, Science **289**, 602 (2000).

¹⁰ S. Uryu and T. Ando, Phys. Rev. B **72**, 245403 (2005).

¹¹ J. W. G. Wilder, L. C. Venema, A. G. Rinzler, R. E. Smalley, C. Dekker, Nature **391**, 59 (1998).

¹² Here we focus on momentum conservation along the tubes, which is all that is conserved in the case of the rope geometry. We defer a discussion of rotational symmetry in multiwall tubes to §IID.

¹³ T. Nakanishi and T. Ando, J. Phys. Soc. Japan **70**, 1647 (2001).

¹⁴ D.-H. Kim and K. J. Chang, Phys. Rev. B **66**, 155402 (2002).

¹⁵ S. Datta, *Electronic transport in Mesoscopic Systems*, 2 ed. (Cambridge University Press, 1995).

¹⁶ A. Hansson, M. Paulsson, and S. Stafström, Phys. Rev. B **62**, 7639 (2000).

¹⁷ H. J. Choi, J. Ihm, S. G. Louie, and M. L. Cohen, Phys. Rev. Lett. **84**, 2917 (2000).

¹⁸ L. Chico, L. X. Benedict, S. G. Louie, and M. L. Cohen, Phys. Rev. B **54**, 2600 (1996).

¹⁹ M. Igami, T. Nakanishi, and T. Ando, J. Phys. Soc. Jpn. **68**, 716 (1999).

²⁰ This result is in contrast to the results in Ref. 18, where it was suggested that the conductance at $E = 0$ grows with the circumference of the carbon nanotube.

²¹ Our results on the discrete lattice sample length at the values $L = \mu a$ with μ integer, thus there is an arbitrary offset of π/a .

²² J. Cumings and A. Zettl, Phys. Rev. Lett. **93**, 086801 (2004).

²³ A. Hansson and S. Stafström, Phys. Rev. B **67**, 075406 (2003).

²⁴ C. Buia, A. Buldum, and J. P. Lu, Phys. Rev. B **67**, 113409 (2003).

²⁵ R. Tamura, Y. Sawai, and J. Haruyama, Phys. Rev. B **72**, 045413 (2005).

²⁶ Q. Yan, J. Wu, G. Zhou, W. Duan, and B.-L. Gu, Phys. Rev. B **72**, 155425 (2005).

²⁷ J. Kim, J.-R. Kim, J.-O Lee, J. W. Park, H. M. So, N. Kim, K. Kang, K.-H. Yoo, and J.-J. Kim, Phys. Rev. Lett. **90**, 166403 (2003).

²⁸ S. Frank, P. Poncharal, Z. L. Wang, and W. A. de Heer, Science **280**, 1744 (1998).

²⁹ T. Kostyrko, M. Bartkowiak, and G. D. Mahan, Phys. Rev. B **60**, 10735 (1999).

³⁰ C. T. White and T. N. Todorov, Nature **393**, 240 (1998).

³¹ R_s is one half of the total reflection coefficient. Given that there are two incoming modes, it can be interpreted as the average reflection probability for each mode.

³² Owing to uncertainties in the experimental parameters we cannot rule out some contribution of deformations of the outer shell (which will act to reduce the ratio R_s/I_s) in addition to potential defects.

³³ Here α and β are restricted to the two atomic positions on the edge of the armchair nanotube of differing local symmetry.

³⁴ For a review see K. Schönhammer, in “Interacting Electrons in Low Dimensions” Ed. D. Baeriswyl, (Kluwer Academic Publishers, 2004); cond-mat/0305035.

³⁵ M.A. Tunney, PhD thesis, University of Cambridge (2005).

³⁶ R. Egger, Phys. Rev. Lett. **83**, 5547 (1999).